Available online at www.sciencedirect.com
ScienceDirect
Nuclear Instruments and Methods in Physics Research A 589 (2008) 350–361
NUCLEAR INSTRUMENTS & METHODS IN PHYSICS RESEARCH Section A
www.elsevier.com/locate/nima

Amplitude calibration of a digital radio antenna array for measuring cosmic ray air showers

S. Nehls[a,*], A. Hakenjos[b], M.J. Arts[c], J. Blümer[a,b], H. Bozdog[a], W.A. van Cappellen[c], H. Falcke[c,d], A. Haungs[a], A. Horneffer[d], T. Huege[a], P.G. Isar[a], O. Krömer[e]

[a]*Institut für Kernphysik, Forschungszentrum Karlsruhe, 76021 Karlsruhe, Germany*
[b]*Institut für Experimentelle Kernphysik, Universität Karlsruhe, 76021 Karlsruhe, Germany*
[c]*ASTRON, 7990 AA Dwingeloo, The Netherlands*
[d]*Department of Astrophysics, Radboud University, 6525 ED Nijmegen, The Netherlands*
[e]*Institut für Prozessdatenverarbeitung und Elektronik, Forschungszentrum Karlsruhe, 76021 Karlsruhe, Germany*

Received 13 September 2007; received in revised form 19 February 2008; accepted 19 February 2008
Available online 5 March 2008

Abstract

Radio pulses are emitted during the development of air showers, where air showers are generated by ultra-high energy cosmic rays entering the Earth's atmosphere. These nano-second short pulses are presently investigated by various experiments for the purpose of using them as a new detection technique for cosmic particles. For an array of 30 digital radio antennas (LOPES experiment) an absolute amplitude calibration of the radio antennas including the full electronic chain of the data acquisition system is performed, in order to estimate absolute values of the electric field strength for these short radio pulses. This is mandatory, because the measured radio signals in the MHz frequency range have to be compared with theoretical estimates and with predictions from Monte Carlo simulations to reconstruct features of the primary cosmic particle. A commercial reference radio emitter is used to estimate frequency dependent correction factors for each single antenna of the radio antenna array. The expected received power is related to the power recorded by the full electronic chain. Systematic uncertainties due to different environmental conditions and the described calibration procedure are of order 20%.

PACS: 95.55.Jz; 95.90.+v; 98.70.Sa

Keywords: Cosmic rays; Air showers; Radio antenna array; Electric field strength; Calibration

1. Introduction

Since Viktor Hess discovered the existence of cosmic rays in the early 20th century, there have been many different experiments and methods for the measurement of this radiation. These cosmic rays consist mainly of ionized atomic nuclei originating mostly from extra-solar sources with energies from a few 10^9 eV to above 10^{20} eV. The measurements of these particles are based on two different techniques. In the energy range up to 10^{14} eV direct measurements in space or with balloons are possible. Above this energy, it is necessary to use the so-called indirect methods. Here, one measures the resulting particle shower when a cosmic ray nucleus interacts with nuclei of the air molecules. The first high-energy interaction at higher altitudes is followed by a cascade of secondary interactions, which creates an extended disc of particles. This shower disc consists of a hadronic component (approximately 1% of the shower particles at sea level), muons (approximately 10%), and an electromagnetic component (electrons and positrons approximately 90%) [1].

Beside generating these secondary particles, the interaction of the electromagnetic component of the shower with the surrounding medium causes secondary radiation based

*Corresponding author.
E-mail address: steffen.nehls@ik.fzk.de (S. Nehls).

0168-9002/$ - see front matter © 2008 Elsevier B.V. All rights reserved.
doi:10.1016/j.nima.2008.02.092

on different mechanisms. Excitation of nitrogen atoms in the atmosphere leads to fluorescence radiation and ultra-relativistic electrons and positrons emit Cherenkov radiation, both at a few hundred nanometers wavelength. For radiation in the radio frequency range the origin is most likely connected with the Earth's magnetic field, already suggested in the late 1960s by Hazen et al. [2] as geomagnetic production. In the early 1970s experiments measured the radio pulses in EAS and could verify the order of magnitude for the absolute field strength. These experiments were summarized in an excellent review of Allan et al. [3]. Nevertheless there was a lack of understanding of the theory for the geomagnetic effect, leading to large uncertainties for the detected radio pulses [4].

In 2003, Falcke and Gorham [5] considered the radiation as a coherent geosynchrotron effect which is a result of electron–positron pairs being deflected in the terrestrial magnetic field and emitting synchrotron radiation. Taking into consideration the overlap of different pulses and the properties of the shower, the results are several tens of nanosecond long radio pulses. They can be measured nearly unattenuated at ground level. Within this framework of the geosynchrotron effect, values for the electric field strength at ground level were predicted, first with analytical [6], and later with full Monte Carlo calculations [7]. By these simulations it was proposed that the field strength emitted by air showers with primary energies above 10^{17} eV should be detectable by an antenna array like the LOPES experiment [8].

The LOPES digital radio antenna field of 30 east–west polarized short dipole antennas is placed inside the existing multiple detector-component air shower experiment KASCADE-Grande [9,10] and measures the radio pulse emitted by the particle shower. But, to finally compare the measured pulses with expectations from detailed simulations the measured amplitudes of the antennas have to be calibrated, i.e. the conversion factor from ADC counts to electric field strength amplitude per bandwidth in ($\mu V\,m^{-1}\,MHz^{-1}$) has to be estimated.

This paper describes a method for an almost complete end-to-end amplitude calibration of an antenna array like LOPES. The purpose of LOPES is the measurement of the absolute electric field strength of radio pulses emitted by extensive air showers.

2. The LOPES antenna array

The LOfar PrototypE Station—LOPES consists of 30 dipole antennas distributed over the field of the KASCADE-Grande experiment in the Forschungszentrum Karlsruhe, Germany. The antennas were designed as prototypes for the LOFAR experiment [11], a large antenna array for astronomical purposes. LOFAR is presently being built in The Netherlands. The initial idea for LOPES was to test the potential of the LOFAR setup for the measurement of cosmic rays and to investigate the properties of the radio component of an extensive air shower. A related experiment, CODALEMA [12], at the Nançay radio observatory is also investigating this radio component.

The aim of the LOPES experiment is to correlate the observables of the radio measurements with the shower properties provided by the particle air-shower experiment KASCADE-Grande. For this reason LOPES is triggered by KASCADE-Grande and uses the reconstructed shower data as input for the pulse analysis. In other words, the shower core position at ground and the direction of the shower axis are used as starting values for the reconstruction of the radio signals. A layout of the experimental setup is sketched in Fig. 1. KASCADE-Grande consists mainly of stations equipped with scintillation detectors, where 252 stations compose the KASCADE array, and further 37 large stations the Grande array. LOPES consists of 30 LOFAR-type antennas as well as newly designed antennas forming the LOPES^{STAR} array [13]. The main purpose of LOPES^{STAR} is to optimize the hardware for an application of this measuring technique to large scales, e.g. at the Pierre Auger Observatory [14]. All antennas are optimized to measure in the relatively noise-free frequency range of 40–80 MHz.

The LOPES antennas are inverted-V dipole antennas, where the angle between the wires is 85°, and the length of the two arms correspond to $\lambda/2$ at 75 MHz. The wires are placed inside plastic tubes for protection. These tubes are standing atop of a metal pedestal to protect them from maintenance works at the KASCADE field. The antennas

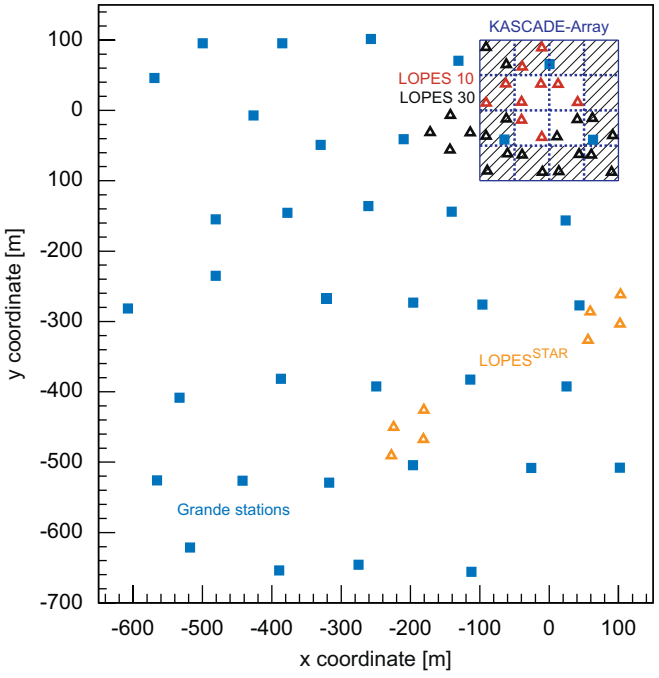

Fig. 1. Sketch of the KASCADE-Grande and LOPES experiments: the KASCADE particle detector array and the distribution of the 37 stations of the Grande array are shown. The location of the 30 LOPES radio antennas as well as the LOPES^{STAR} antennas is also displayed.

are connected to low noise amplifiers (LNAs). The signal is then transmitted via a coax cable to one of the three stations where it is again amplified, filtered and digitized. The three stations with 10 antennas each are operated by independent electronic chains and data acquisition systems. One of these three stations was forming the initial LOPES10 experiment [15]. The data are ring-buffered for 6.25 s and read-out only if an external trigger arrives (from KASCADE-Grande). Then the central DAQ-PC collects 0.82 ms of data around the trigger from all 30 antennas, adding a KASCADE-Grande time-stamp, and stores them as one LOPES-event file. Fig. 2 displays the scheme of the LOPES electronics in more detail.

In Fig. 3 an uncalibrated power spectrum from a LOPES-event file is shown. The narrow band radio emitters exceed the noise floor by orders of magnitude. During the analysis procedure these narrow band radio frequency interferences (RFIs), like from a TV-transmitter as shown in the zoom-in of Fig. 3, are removed. With a RFI mitigation it is possible to strongly suppress most of these narrow emitters, which leads to a better signal-to-noise ratio for the detected radio pulses.

Finally, a beam-forming procedure is applied to search for coherent peaks coming from a specific direction. This digital beam-forming consists of a time shift of the data according to the given direction and afterwards a combination of the data to calculate the resulting beam from all antennas. At this point, the reconstructed shower direction from KASCADE-Grande is used as a starting value. For details of the experimental setup of the LOPES radio antennas see Refs. [8,15,16].

First analysis results of the measurements with the LOPES10 setup have already been published [15,17–19].

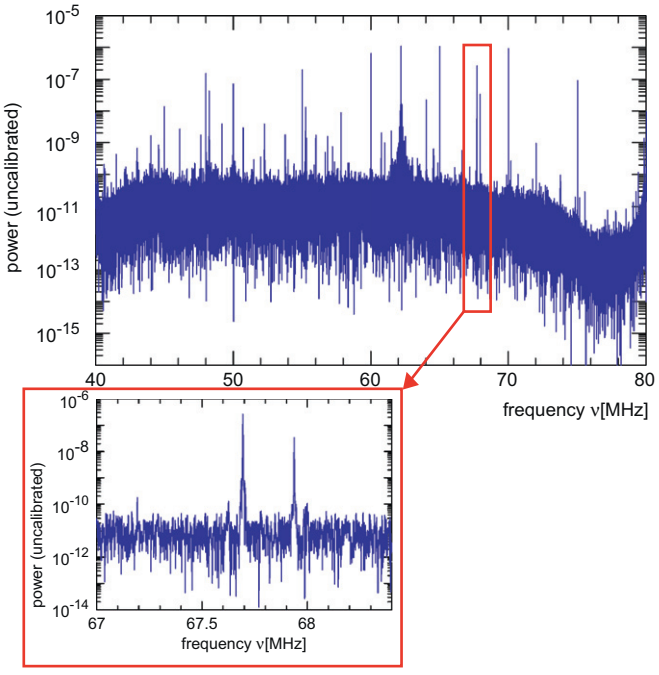

Fig. 3. Typical, uncalibrated LOPES raw signal in the frequency domain. The zoom-in shows two audio signal carriers from a TV-transmitter at 67.70 and 67.92 MHz in more detail.

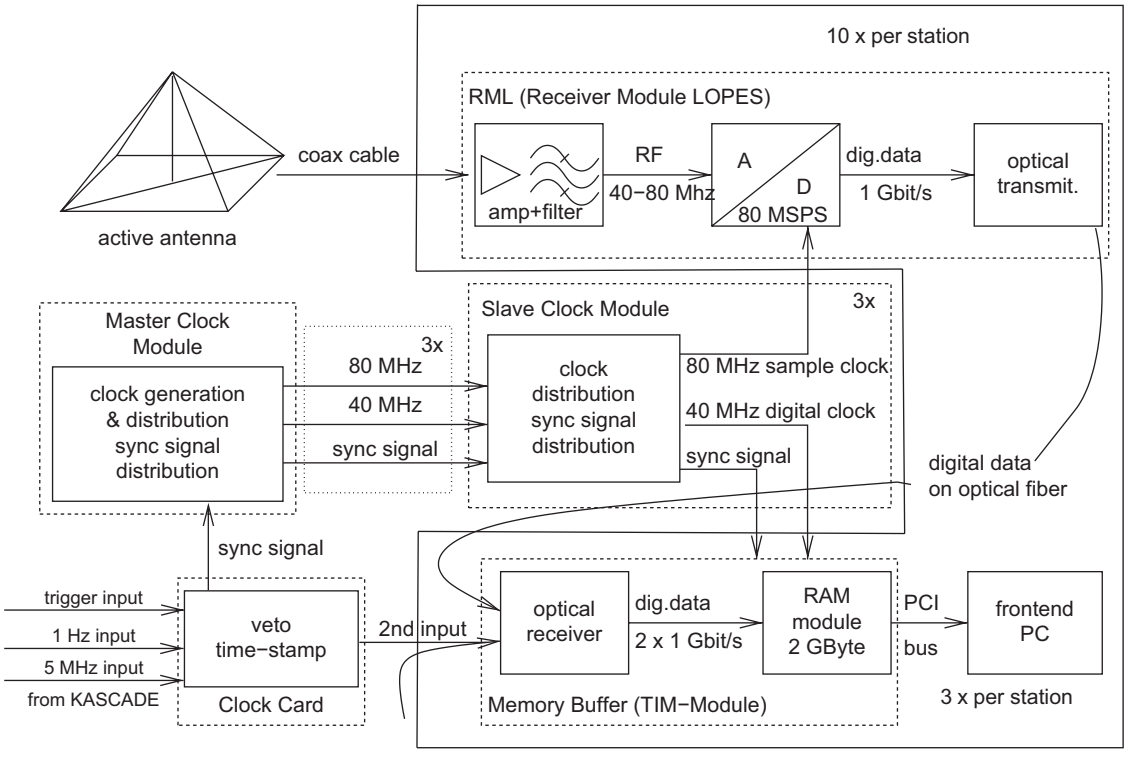

Fig. 2. Scheme of LOPES electronics: incoming radio pulses from EAS are received with the active antenna and transmitted via a long coax cable (RG-213) to the Receiver Module (RML). The amplified and bandpass filtered analog signals are digitized with a 12-bit A/D converter. After the optical fiber transmission the signals are stored in a memory buffer. Trigger from KASCADE-Grande are distributed by a master clock module to each station and finally transmitted to the front-end PC for data read-out.

All the results published so far, however, rely on relative field strength values, which were only roughly normalized by a fudge factor. To quantify the measurements and to compare with theoretical expectations the antennas need the absolute amplitude calibration.

3. Amplitude calibration

Compared to the smaller initial LOPES10 setup with only one DAQ-station, for the LOPES30 setup larger variations in the behavior of the individual electronic channels can be expected. Therefore, a relative measure of the electric field strengths, as it was done for the initial LOPES10 setup, is not sufficient. Instead, an amplitude calibration has to be performed for the whole setup, including the full electronic chain of the antenna, i.e. LNA, cable, filter, and analog-to-digital converter.

In general, to perform an amplitude calibration of the antennas there are two possibilities: either the antenna characteristics are calculated theoretically and the electronic chain is calibrated in the laboratory or the full chain is calibrated by an external source of known field strength. The former method was performed for the LOPES10 configuration and has only applicability for relative comparisons of radio emission and air shower properties. The latter procedure has the advantage of calibrating the full chain of the experiment, the antenna and the electronics simultaneously (end-to-end calibration). In addition, this approach provides the opportunity to investigate influences of environmental variables such as weather or ground humidity during shower measurements and to test the simulated antenna gain pattern.

For LOPES30 we have chosen a combination of end-to-end calibration with the determination of the behavior of individual components. This hybrid method requires an antenna gain simulation. A full experimental test of these simulation results requires dedicated measurements, which are partially performed for this analysis. As external source for a calibration one can either use an astronomical one, like the galactic background radiation [20], or a man-made radio source. For the location of the LOPES-experiment the galactic background radiation is fully oblique due to man-made noise sources at Forschungszentrum Karlsruhe and can therefore not be used as reference source. What follows is the description how LOPES30 is amplitude calibrated with the help of an external reference source.

3.1. Method

The amplitude calibration is based on two ingredients: First, in each individual antenna the signal received from a calibrated radio source is measured. Second, the expected signal to be received is calculated using antenna characteristics obtained from simulations. Then, we compare the expected signal strength with the measured signal and derive a amplification factor as the ratio of measured to expected signal, describing how the system alters the incoming signals.

The main characteristic of the antenna is defined by its directivity. This directivity describes the reception or emission features for each direction in relation to a mathematical reference antenna like the ideal isotropic radiator. The ratio between the power received by a real antenna and the ideal isotropic radiator for a given direction is called antenna gain G. This antenna gain can be obtained by measurements or simulations. Experience within the LOFAR initial test station (ITS [21]) has shown that the measurements contain larger uncertainties than the simulations. Therefore, the calibration is mainly realized for the zenith direction. For other directions we will rely basically on simulations. Nevertheless, some test measurements are performed to verify the simulated values of the full directivity as the method allows to measure the full direction characteristics and to evaluate the antenna gain simulation (Section 4.5).

The method is based on the fact, that the frequency dependent electric field strength $E_t(\nu)$ at a certain distance is known. This electric field strength can also be expressed as known output power $G_tP_t(\nu)$ of the commercial radio source. The commercially calibrated radio source is used as emitter which LOPES measures within a calibration mode from artificially triggered events. The simulated antenna gain G_r of the LOPES antennas is an input value for the calculation of the power which is received by the LOPES electronics. This calculated input power $P_{\mathrm{R}}(\nu)$ is compared with the measured power $P_{\mathrm{M}}(\nu)$. The result is a frequency dependent amplification factor $V(\nu)$ which will be used during the analysis of the LOPES air shower data to calculate the absolute field strength:

$$V(\nu) = \frac{P_{\mathrm{M}}(\nu)}{P_{\mathrm{R}}(\nu)} = \left(\frac{4\pi r\nu}{c}\right)^2 \frac{P_{\mathrm{M}}(\nu)}{G_r(\theta,\phi,\nu)G_tP_t(\nu)\cos^2(\beta)} \qquad (1)$$

with

- P_{M} The power measured with the LOPES antenna and calculated in the frequency domain.
- P_{R} The (calculated) incoming power to the LOPES electronics chain.
- ν Frequency of the emitted signal.
- r Distance between the external reference source and the LOPES antenna.
- $G_r(\theta,\phi,\nu)$ Gain of the LOPES antenna taken from simulations.
- $G_tP_t(\nu)$ Product of the reference source antenna gain G_t and its power P_t which are not exactly known by themselves, but known as the electric field strength $E_t(\nu)$ in $r = 10\,\mathrm{m}$ distance. This value is obtained from the manufacture calibration report of our reference source.
- β Angle between the polarization axis of the reference source and the field antenna. This axis has to be aligned during the measurements.

3.2. Simulation of the antenna gain

The simulations were performed with the program package IE3D from Zeland company (see also www.zeland.com), a program using the multi-pole expansion to calculate the electromagnetic properties of three-dimensional antennas. As input to the simulations the real geometry of the LOPES antenna including the metal pedestal is used. The inverted-V dipole of the LOPES antenna has an opening angle of $\alpha \approx 85^\circ$ which alters the directivity pattern compared to a linear dipole. Taking into account that at 75 MHz it represents a $\lambda/2$ dipole the directivity pattern is determined. For the definition of the ground an infinite plane is assumed and the electrical properties of this ground plane are similar to the real ground. Therefore resistance, ground humidity, and conductivity are chosen to be close to the actual condition at the antenna field. For the dielectric constant the value was set to $\varepsilon_r = 3$ and a value of $\sigma = 0.01\,\mathrm{S\,m^{-1}}$ was used for the conductivity. The simulation describes only the antenna itself, and therefore no antenna coupling was considered. Hence, a possible effect of mismatch cannot be seen directly from the simulations, but will be taken into consideration automatically by our method of end-to-end amplitude calibration. The simulation ranges from 10 to 100 MHz and results in a gain value for each frequency (1 MHz step size) and direction (zenith angle θ with 5° and azimuth angle ϕ with 10° step size) of the incoming signal, which can be displayed as a directional diagram.

In Fig. 4, a vertical cut through the simulated diagram is shown and the antenna gain $G_r(\theta, 180^\circ, \nu)$ is displayed for different frequencies. The gain is expressed as a relative value to the sensitivity of an isotropic radiator. The main lobe of the antenna has −3 dB angle of ≈ 70°. Side lobes are strongly suppressed due to the pedestal of the LOPES antenna and the ground plane conditions. This −3 dB angle is the full-width half-maximum (FWHM) angular beam width. For zenith angles θ above 60° the gain drops significantly compared to the line of symmetry (in the zenith, $\theta = 0^\circ$).

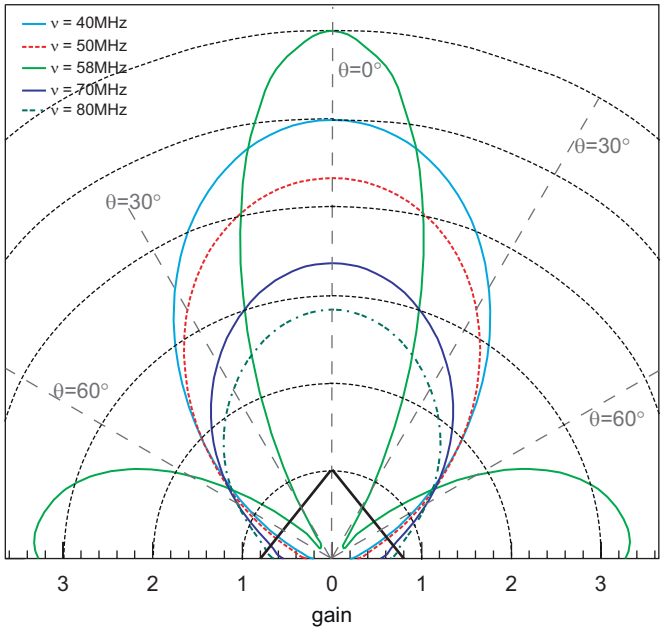

Fig. 4. Antenna gain $G_r(\theta, 180^\circ, \nu)$ of the LOPES antenna in the $\vec{E}$-plane (zenithal sensitivity). The antenna illustrated by a triangle in the center of the x-axis lies in the image plane.

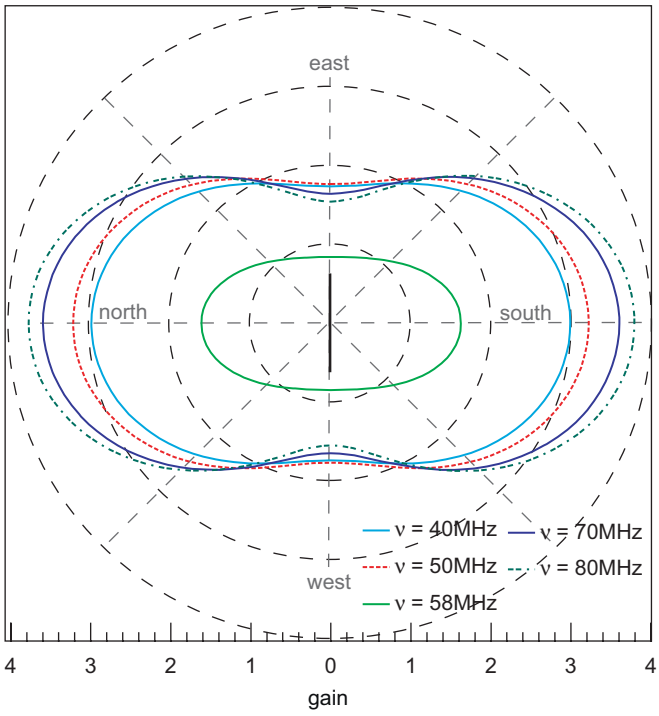

Fig. 5. Antenna gain $G_r(45^\circ, \phi, \nu)$ of the LOPES antenna for a fixed zenith angle (azimuthal sensitivity). This can be considered as a horizontal plane cut at $\theta = 45^\circ$ in Fig. 4. The dipole antenna lies on the y-axis.

In Fig. 5, a horizontal cut through the simulated diagram at a fixed zenith angle of $\theta = 45^\circ$ is shown. The visible main lobes at such a zenith angle display an oval shape and the dipole origin is only indicated by the constriction along the y-axis at gain zero on the x-axis. It is obvious that the antennas prefer radio pulses from north or south as a result of its orientation (i.e. here the east–west direction).

An interesting feature is the behavior at 58 MHz, visible as horizontal side lobes in Fig. 4. The simulations indicate that there is a resonance induced from the 2 m × 2 m metal pedestal below the antenna. The resonance seems to be sharp and should be visible in the calibration procedure but will be checked by specific measurements (Section 4.5).

3.3. The reference antenna

The discussed calibration method relies on an external radio source which is calibrated independently. For the actual amplitude calibration method a commercial product from the company Schaffner, Augsburg (Type: VSQ 1000 with DPA 4000 and RSG 1000) was used (see also data sheets at www.teseq.com or Ref. [22]).

Fig. 6. The VSQ 1000 from Schaffner consists of the signal generator RSG 1000 and the biconical antenna DPA 4000. The total length of the biconical antenna is 40.5 cm (image courtesy of Schaffner).

The setup (VSQ), see Fig. 6, consists of a biconical antenna, Schaffner DPA 4000, attached to a signal comb-generator RSG 1000 which gives a signal peak at multiples of 1 MHz from 1 MHz to 1 GHz. The signal generator has a mean power of 1 μW over the whole LOPES frequency range (40–80 MHz). Since it is battery-operated, it is usable for measurements on the antenna field. The biconical antenna DPA 4000 is linearly polarized and has a nearly constant directivity close to its main lobe. This is important since it results in only a small loss should the radio source be slightly off target. The DPA 4000 is originally designed for the frequency range 300–1000 MHz, but the VSQ 1000 is specified and certificated for the broader frequency range from 30 to 1000 MHz despite the fact that the antenna factor changes in the lower frequency range. Nevertheless, it fits within the LOPES frequency range.

The reference radio source itself is calibrated, hence the resulting field strength at any given distance can be calculated. For the fiducial distance of 10 m from the VSQ the electric field strength ranges from $210\,\mu V\,m^{-1}\,MHz^{-1}$ at 40 MHz up to $2100\,\mu V\,m^{-1}\,MHz^{-1}$ at 80 MHz. The systematic uncertainty of the calibration measurements for the electric field strength is 2.5 dB (or $\approx 30\%$). This value is reported in the certificate of calibration provided by the manufacturer for our individual VSQ. Beside this uncertainty of the calibration method the signal stability of the RSG 1000 for the temperature range 10–30 °C is <0.5 dB (or $<6\%$). For the analysis the electric field strength is converted into a power $P = 4\pi(r \cdot E[\mu V\,m^{-1}])^2/Z_0$, with $\log_{10}E[\mu V\,m^{-1}] = E[dB\,\mu V\,m^{-1}]/20$ and $Z_0 = 377\,\Omega$.

3.4. Measurements

For a calibration campaign, the whole setup of the VSQ is placed at $r = 10.5$ m above each LOPES field antenna, using a movable crane with a wooden extension

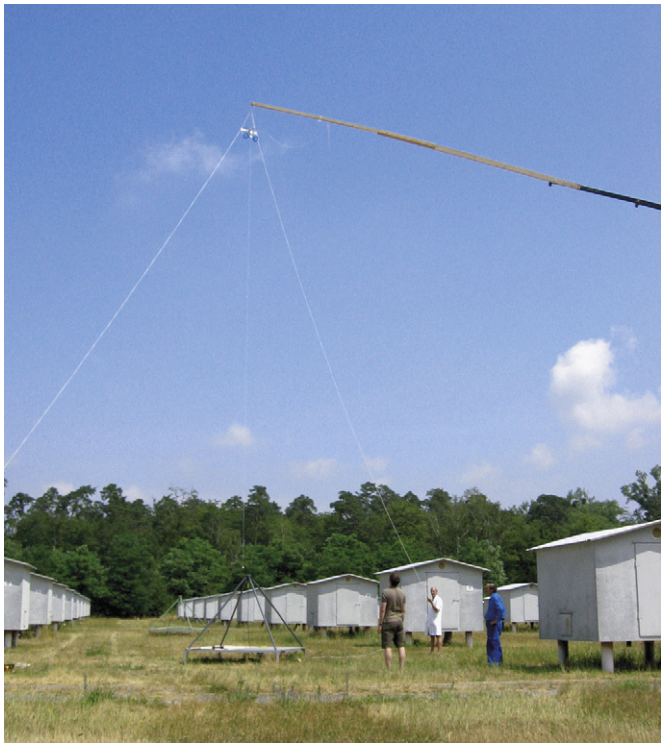

Fig. 7. Calibration campaign at the LOPES field.

(see Fig. 7). Fixed in a frame, the whole setup consists of the reference source VSQ, an external GPS antenna, and the GPS hand-held unit. The wooden extension is necessary to avoid reflections of the radio signal off metal parts of the crane, which would otherwise lead to differences between calculated and real received power. For the VSQ setup we use a plummet with a fixed length and a differential GPS to determine the exact position of the radio source. As a calibrated source is used, the power of the radio signal which arrives at the antenna can be calculated. For the LOPES electronics we are using an 80 MHz ADC working in the second Nyquist-domain, digitizing the measured voltages for frequencies from 40 to 80 MHz.

The calibrated external radio source is emitting at a distance of $r = 10.5$ m and the received signal in the field antenna is transmitted to the electronics chain via a long coaxial cable. During each calibration run, artificially triggered data files are stored. Each file contains $N = 65\,536$ samples per antenna, at a sampling rate of 12.5 ns this results in 819.2 μs of data. The calibration setup lasts for at least 2 min at a field antenna and uses a trigger period of 6 s (rate 0.17 Hz), which leads to 20 or more stored data files. This way of data taking is used to average over small geometric variations in the setup. On the other hand, influences from wind gusts and fast changes in environmental conditions can be monitored and affected data files are not considered for the next analysis steps.

Each data file is analyzed individually in our software package and after a Fourier transformation the complex values are used to calculate the amplitude for a certain

frequency. The resolution in the frequency domain from 40 to 80 MHz is determined by the Fourier transformation to $N/2 = 65\,536/2 = 32\,768$ bins to $40\,\text{MHz}/32\,768 = 1.22$ kHz. The characteristic of our reference source is a comb-shaped spectrum with 1, 5, or 10 MHz spacing. In nearly all cases the 1 MHz spacing is used to get a high coverage for the LOPES frequency range. An example is shown in Fig. 8. The amplitude in the frequency domain is equivalent to the received power, binned with $N/2 = 32\,768$ bins. The received power $P_M(\nu)$ for each integer frequency is determined by summing over 50 bins or 61 kHz around the center of the peak. The peak value is on average three orders of magnitude higher than the surrounding noise level and has spreads over roughly 5–10 bins, i.e. 6–12 kHz. The noise floor around the frequency peak contributes with less than 1% to the integrated power. At some fixed frequencies, not every time, and not in all antennas, man-made RFI in the same order of magnitude as the received signals affects the measurement. Therefore a linear interpolation of the received power replaces these contaminated frequencies.

The integrated power P_M for each integer frequency averaged over all data files in a calibration step (at least 20 events in 2 min) reflects the overall behavior of the LOPES antenna system during such a measurement. For each antenna a set of measurements $P_M(\nu)$ exists, which is used to calculate the ratio $V(\nu)$ of measured to expected power.

For that purpose one has to be sure that one operates in the far field region, not to be disturbed by near field effects of the emitter. The far field approximation ($r_{far} > 2D^2\nu/c$) should be valid for $r_{far} > 2$ m at 80 MHz and with an antenna aperture $D = 1.8$. In the far field approximation the energy density of the electromagnetic field varies as r^{-2} with the distance r. Fig. 9 shows measurements of the received power P_M with respect to the distance r between the reference source and the LOPES antenna. The power P_M is the integrated power over 61 kHz around the mean frequency. For distances of $r = 4.5$–11.5 m the far field approximation was tested. As the fits for the different frequencies (51, 56, and 61 MHz) are performed with a fixed power index of -2, $P = a \cdot r^{-2}$, the measurement clearly shows the validation of the far field approximation. This measurement has also shown that a possible saturation effect for the low-noise amplifier is unlikely, and that the calibration acts in the linear working regime. The 12-bit ADC also does not suffer from a saturation effect, but the closest measurement at 4 m distance was at the limit of analogue input voltages (±1 V) for the ADC. For the calibration campaigns a distance r between field antenna and reference source of around 10 m was chosen, therefore, we can exclude saturation effects for the determination of the amplification factors.

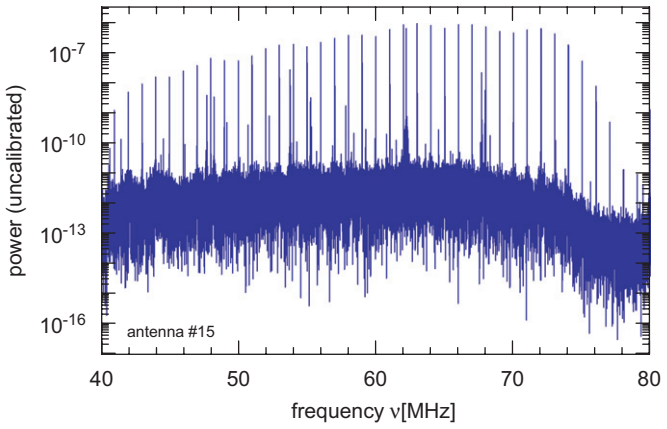

Fig. 8. Measured power of one calibration raw data file. Clearly visible are the 1 MHz steps of the emission of the reference antenna.

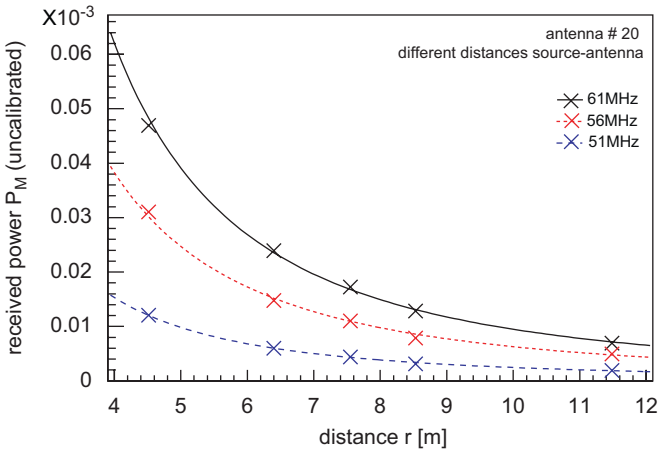

Fig. 9. The data points show the received power P_M integrated over 61 kHz for various frequencies as a function of r, which is the distance source—LOPES antenna. The lines are fits of a r^{-2} dependence.

4. Results

4.1. Amplification factors

The amplification factors $V(\nu)$ for all 30 LOPES antennas are shown in Fig. 10. The curves for each antenna represent the mean values of measurements performed over two years. The frequency range of the ADC is between 40 and 80 MHz, however, also the filter characteristics at the upper and lower bound can be seen, which gives an effective range of approx. 44 to approx. 75 MHz. The difference in the shape of the individual antenna amplification curves is a result of different types of filters and batches of electronic components installed for the first 10 antennas compared to the later installed antenna setups. At the actual configuration of LOPES the cable length is either 100 or 180 m, which might also lead to differences in the amplification factors for different antennas. But it was found that the total scatter between the amplification factors (Fig. 10) does not simply relate to the cable length. Instead, the scatter originates roughly to equal parts from the adjustments of the operating points of the electronic modules, peculiarities for certain antenna field positions, and the different cable lengths.

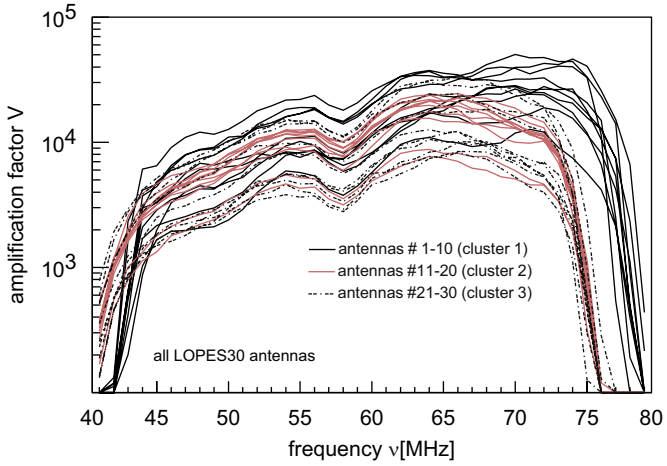

Fig. 10. Amplification factors of all LOPES antennas. The different colors and line types are used to separate the three antenna clusters. Each cluster combines 10 antennas with their individual electronics.

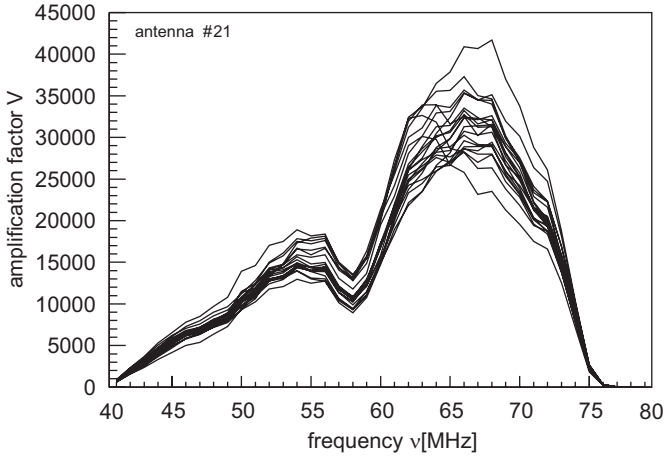

Fig. 11. Amplification factor of one LOPES antenna for independent measurements. These measurements were spread over the course of nearly two years and include 21 calibration campaigns.

A common feature of all curves in Fig. 10 is a dip at 58 MHz. This feature relates to the antenna gain simulation and is described in more detail in Section 4.5.

The large overall scatter between the individual antennas of roughly one order of magnitude obviously necessitates the complete amplitude calibration. In the analysis of the shower data we use the amplification factors to correct the raw data in order to get calibrated power values. Moreover, related systematic effects in the determination of these amplification factors $V(\nu)$ have been investigated, which will be described in the following sections.

4.2. Stability of the calibration

An important issue of the calibration procedure is its stability over repeated measurements. Besides uncertainties in the position or the alignment of the reference source with the field antenna or by small changes in handling the experimental calibration procedure (see Section 4.4), there could be large differences between the measurements of an antenna due to changing environmental conditions like precipitation, ground humidity, air temperature, etc. If such differences exist to a greater extent, this would cause problems in the applicability of the amplification factors. To verify the influence of such changing environmental conditions we performed a series of measurements over roughly two years. In these campaigns one field antenna (antenna #21) was measured each time and therefore under different environmental conditions. The resulting amplification factors for this antenna are displayed in Fig. 11. The measurements include weather conditions occurring during the year in Karlsruhe, except extremes like snow and thunderstorm. The temperature ranges from around $\sim -5\,^{\circ}$C up to $\sim 35\,^{\circ}$C, the soil change from dry in the surface layer (0–60 cm) to a high ground humidity after days of rain, and the ground vegetation varies from recently mowed to a flowery meadow. The variation found is a measure of the systematic uncertainties of the calibration procedure or, on the other hand, reflects the accuracy of this calibration method. In the effective frequency range of the LOPES bandpass filter from 44 to 75 MHz an average scatter of about 9% was found.

It is obvious that the variation from antenna to antenna (Fig. 10) is much larger than the variation due to changing environmental conditions or conditions of the calibration procedure (note the logarithmic scale in Fig. 10 compared to the linear scale in Fig. 11).

There are many possible sources for the systematic uncertainties and a significant reduction of the observed variation requires deeper investigations. One possible source of the variations is thought to be the LNA temperature. But the temperature of the LNA at the antenna and at one end of the long coaxial cable is not directly available. The remaining part of the cable and the LOPES electronics is either underground or inside an air-conditioned housing. However, variations with the air temperature can be used as a first order approximation. We use the air temperature at two meters height above ground, which is provided by the KASCADE experiment. With 24 h continuous monitoring using the VSQ at a fixed position in a distance of 16.5 m and with a zenith angle of 87°, we covered an air temperature range of 3–28 °C. The data taking is similar to the calibration campaigns, except that here the KASCADE trigger is used, with an average rate of 0.04 Hz. For each 10 min an averaged amplification factor $V(\nu)$ is calculated. Fig. 12 displays the average amplification factor $V(73\,\text{MHz})$ (squares, left y-axis) and the air temperature in degrees at 2 m height (circles, right y-axis) over time. To show the relative change of the average amplification factor, the highest value at the day was used for normalization. The daily temperature modulation is well pronounced and shows a minimum in the early morning. The highest temperature was recorded in the early afternoon. As the performance of electronic devices changes with temperature, the LNA circuit

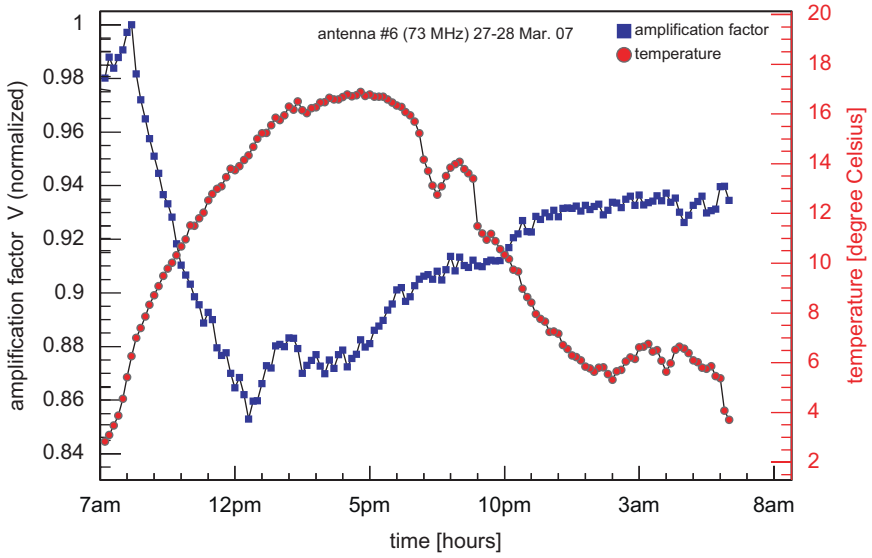

Fig. 12. Amplification factor of antenna 6 at 73 MHz (left y-axis) and temperature 2 m above ground (right y-axis) plotted against time. The antenna was monitored over a period of 24 h with fixed setup started at 7 a.m. and the highest value was used to normalize the amplification factor V. The maximum drop for V is obtained at 12 p.m. and add up to around 15%.

connected directly to the antenna at the field has a better performance at low temperature values.

From Fig. 12 one derives that in general the amplification factor decreases to lower values with increasing air temperature. The maximum drop add up to around 15% for the amplification factor at this day and is obtained at 12 p.m. For the covered air temperature range one can derive that 10° difference in temperature causes a change of about 10% in the amplification factor. This implies that a first order correction of this effect is possible using the air temperature. The uncertainty in temperature stability of about 6% of the reference signal generator is not corrected for. This value is considered for the temperature range 10–30 °C. The change in temperature is somewhat higher than this methodical uncertainty, but cannot be disentangled. Nevertheless, the LNA temperature should be measured directly to fully verify the temperature dependence of the LOPES system.

4.3. Cross-check of the polarization sensitivity

Since the end of 2006 LOPES is operating some antennas in a dual-polarized configuration. In particular, for such a configuration a cross-check of the polarization sensitivity has to be performed during the calibration campaigns. Fig. 13 shows the relative amplification factors for the east–west oriented antenna #5 measured in one campaign where the azimuth angle ϕ was varied in steps of 10° by rotating the VSQ reference source above the field antenna ($\phi_{\mathrm{Ant}} = 90°$, equal to east–west orientation). The amplification factor V at $\phi = 90°$ was used for normalization. From formula (1) we know that the received power changes with $\cos^2\beta$, with respect to the linear polarized LOPES antenna. The angle β is defined as the angle between the axes of VSQ and field antenna. The azimuth angle ϕ is related with the angle β by $\phi = \beta - \phi_{\mathrm{Ant}}$.

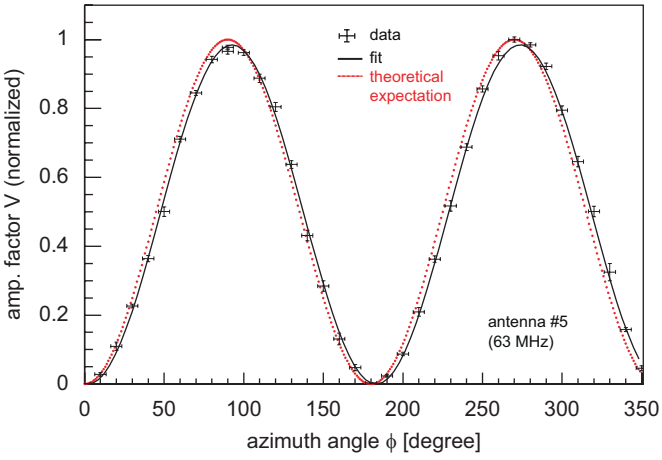

Fig. 13. Relative amplification factors V at 63 MHz for the dual-polarized antenna 5, but with varying the azimuth angle ϕ and normalized to the amplification factor at $\phi = 270°$. The position of the source was vertical above the LOPES antenna. The fitted function $V(\phi) = a \cdot \cos^2(\phi + \alpha - \phi_{\mathrm{Ant}})$ is indicated by a black line and the theoretical expectation $V(\phi) = \cos^2(\phi - \phi_{\mathrm{Ant}})$ by a red dashed line, both are normalized to the value at $\phi = 270°$.

The result obtained in Fig. 13 prove the expected $\cos^2\beta$ polarization sensitivity of the LOPES antenna, here exemplarily shown at 63 MHz. The fitted function $V(\phi) = a \cdot \cos^2(\phi + \alpha + \phi_{\mathrm{Ant}})$ uses two free parameter $a = 0.98 \pm 0.01$ as scaling parameter and $\alpha = -3.0° \pm 0.6°$ as angle offset to describe the measurements. The theoretical expectation is based on a $V(\phi) = \cos^2(\phi + \phi_{\mathrm{Ant}})$ with no free parameters. Both curves are very close to each other and show the achieved accuracy for aligning the polarization axes from VSQ and field antenna. With a systematic offset of $\alpha = -3.0°$ for this measurement we derive a

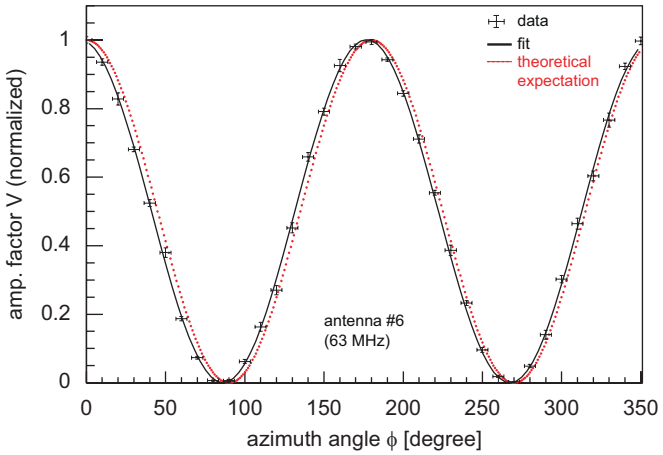

Fig. 14. Same as Fig. 13, but for the perpendicular oriented antenna 6, i.e. an antenna sensitive to the north–south polarization of the signal. Here the fitted function and theoretical expectation are normalized to the value at $\phi = 180^\circ$.

systematic uncertainty of $\sigma_\beta = 7^\circ$. However, in the case of strong disturbing wind the alignment might be worse and can result in a higher loss in the received power.

Fig. 14 shows results of the same measurements at the same antenna station, but the data are analyzed for the north–south oriented antenna #6, i.e. $\phi_{\mathrm{Ant}} = 0^\circ$. Together with Fig. 13 the two plots show the capability and applicability of calibration and event data taking with LOPES in a dual-polarized antenna mode. The measured power ratio of antenna #6 to antenna #5 is less than 2% for the relevant frequency range. Despite this independent calibration there remains the possibility of cross-talk between both channels as their LNAs are mounted in the same box.

4.4. Uncertainties

In previous sections systematic effects of the calibration source, the temperature dependence, and the polarization sensitivity were described. In this section we will discuss in detail the different sources of uncertainties and summarize them. The statistical uncertainty of the calibration procedure for the amplification factors $V(\nu)$ in the effective frequency range 44–75 MHz are in most cases negligible ($\mathrm{stat}_{\mathrm{calib}} = 1.5\%$) due to the 20 'trigger'-measurements per individual calibration configuration.

The total systematic uncertainty for one calibration campaign is estimated by a combination of the individual sources. These sources are identified and the resulting standard deviations estimated for:

- r The uncertainty in estimating the distance between reference source and antenna is estimated to $\sigma_r = 0.25\,\mathrm{m}$.
- ν The deviation in frequency is given by the resolution of the power spectrum after fast Fourier transformation and results to $\sigma_\nu = 600\,\mathrm{Hz}$.
- $G_t P_t$ The information from the data sheet of the reference antenna allows only to estimate the uncertainty of the product of gain and power. There is a variation of the output power with changing temperature in the order of $\sigma_{G_t P_t}/G_t P_t = 12\%$. This does not include the systematic uncertainty for the calibration of the reference source itself, which is 2.5 dB for the electric field, respectively, $\mathrm{sys}_{\mathrm{reference}} \approx 67\%$ for the emitted power.
- G_r The simulated antenna gain. This is second largest source of uncertainty and the largest for the calibration procedure itself and is estimated to be $\sigma_{G_r}/G_r \approx 15\%$, but can be even larger at the expected resonant frequency; see next section.
- P_{M} The uncertainty of the measured power is given by the data acquisition system and read-out process of the power values and estimated to be $\sigma_{\mathrm{P_M}}/\mathrm{P_M} \approx 5\%$.
- β The uncertainty for the angle between the polarization axis of the reference source and the axis of the LOPES field antenna is estimated to $\sigma_\beta = 7^\circ$, which results in a maximum loss of 2% for the emitted power.
- Environmental effects Due to the fact that the LOPES antenna uses the ground as a reflector, humidity at the ground can influence the values, despite the metal reflector below the antennas. An estimation of this uncertainty is derived from performing measurement campaigns over two years (Fig. 11) and results to $\approx 9\%$. In this uncertainty, effects from the antenna coupling, varying ground conditions, and a temperature changes of the signal generator output are included.

From these systematic uncertainties an overall uncertainty for the amplitude calibration of the LOPES antenna array can be calculated to $\sigma_V/V = 0.70$. This includes the statistical uncertainty $\mathrm{stat}_{\mathrm{calib}}$ and all other uncertainties described above. As these uncertainties are of different kind a separation in three main groups can be done:

$$\left(\frac{\sigma_V}{V}\right)^2 = (\mathrm{stat}_{\mathrm{calib}})^2 + (\mathrm{sys}_{\mathrm{calib}})^2 + (\mathrm{sys}_{\mathrm{reference}})^2 = (0.015)^2 + (0.205)^2 + (0.67)^2. \quad (2)$$

Ignoring the calibration uncertainty given by the commercial radio source with $\mathrm{sys}_{\mathrm{reference}} = 67\%$ the listed systematic uncertainties sum up to $\mathrm{sys}_{\mathrm{calib}} = 0.205$. Here, the antenna simulation and the environmental effects give the largest contributions. By more detailed studies of the antenna directivity the uncertainty $\mathrm{sys}_{\mathrm{calib}}$ might be decreased (Section 4.5).

As the weather and environmental effects are difficult to quantify, a correction of a correlation of the system performance with the temperature (as described in Section 4.2) is not yet performed for the amplification

factors. On the other hand, it will improve the uncertainty for the environmental effects only, which contributes only with $\approx 9\%$.

The dominating factor for the total uncertainty is given by the calibration accuracy of the VSQ 1000 radio source, provided by the manufacturer. Using another reference source would lead to a different, maybe smaller, total systematic uncertainty.

4.5. Cross-check of the antenna directivity

The described calibration procedure also allows us to check at least partly the simulation results (Section 3.2) of the antenna gain pattern. The prediction of a pronounced resonance at 58 MHz caused a dip, visible in Fig. 11, and is introduced by the factor G_r in the calculation of the amplification factors. By moving the source away from the zenith, but tilting the source accordingly to keep the emission and the polarization angles constant, one is able to check the zenithal dependence of the antenna gain. For higher inclinations the amplification factors, i.e. the sensitivity of the antenna, decrease. Fig. 15 shows the amplification factors for one antenna measured at the same campaign but the source located at different zenith angles ($\theta \neq 0^\circ$). Due to the fact that in the calculation of the amplification factor V (see Eq. (1)) the simulated antenna pattern G_r is included, the obtained distribution of the amplification factors in Fig. 15 should be always the same in the range of the uncertainty. This is true for a large range of the frequency band, but not around the frequency of 58 MHz. At this frequency, a resonance effect of the metal ground plate is predicted by the simulations (see Fig. 4).

Fig. 16 shows results of the same measurement, but now V calculated with a fixed antenna gain. Choosing for $G_r(\theta, \phi, \nu) = 4.0$ (value for vertical source position at 50 MHz) the antenna pattern corresponds to an isotropic radiator. If the resonance effect would be present as predicted, a clear peak for vertical positions and a large dip for $\theta = 45^\circ$ should be visible at 58 MHz. As this is not the case we conclude that either the calibration procedure smears out all the effects, which is implausible with the obtained total systematic uncertainty of the calibration or the antenna gain simulation overestimates the effect of the ground plate. In addition, the results shown in Fig. 16 suggest that the resonance is at 62 MHz rather than at 58 MHz and not as sharp as expected by the simulations.

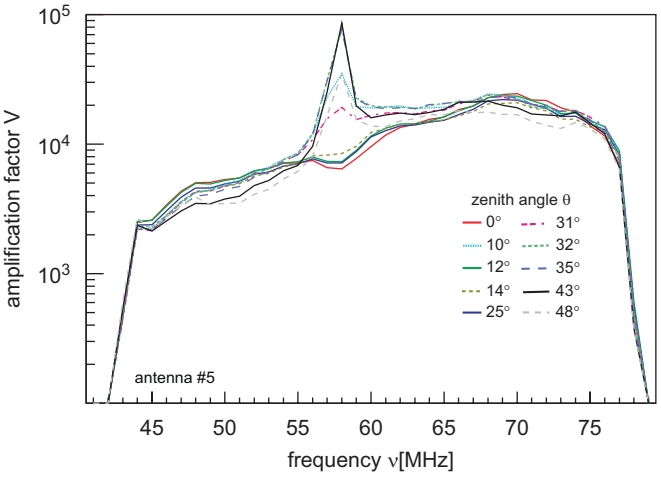

Fig. 15. Amplification factor distributions for one antenna, but calibrated with the reference source located at different distances, i.e. emission in different inclination angles with respect to the LOPES antenna.

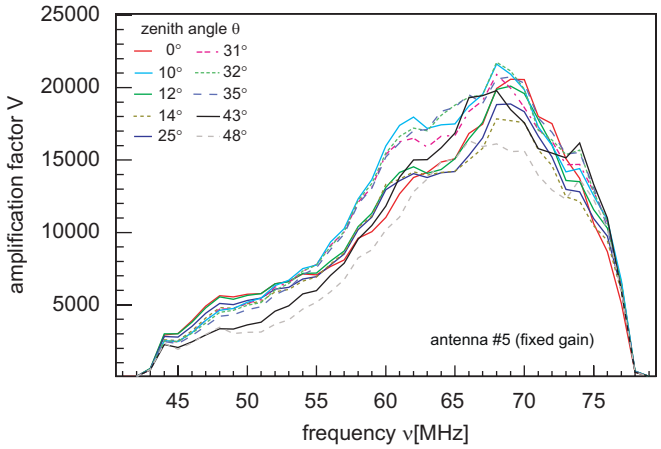

Fig. 16. Same as Fig. 15, but this time the amplification factor V was calculated using a fixed antenna gain $G_r = 4.0$ and plotted with a linear scale for the y-axis.

5. Summary

In this work we studied a method for an absolute amplitude calibration of a digital radio antenna array using a calibrated external reference source. By application of the procedure to the LOPES antenna array we could show that it is possible to derive reliable, frequency dependent amplification factors allowing us to measure the absolute electric field strength emitted by cosmic ray air showers.

The absolute amplitude calibration was successful and detailed investigations of possible systematic uncertainties lead to a total uncertainty of $\sigma_V/V = 70\%$. This total uncertainty also includes e.g. environmental effects, like those caused by different weather conditions present over nearly two years of calibration campaigns ($\text{sys}_{\text{calib}} = 20.5\%$), and a systematic uncertainty from the used reference source ($\text{sys}_{\text{reference}} = 67\%$).

Electronic modules are temperature dependent and we have shown that there is a relation between air temperature and amplification factor $V(\nu)$ for the LOPES antenna system. A more precise correlation analysis and following correction can improve the overall precision for measuring electric field strengths.

The systematic uncertainty of the calibration of the reference radio source itself contributes with $\approx 67\%$ to the total uncertainty. Using another, more precisely calibrated reference radio source would improve the accuracy.

The measurements at a dual-polarized antenna setup with two low noise amplifiers and cables next to each other indicate that a calibration of such a system is possible and reliable. There seems to be no significant cross-talk between the channels. The electric field strength for such a configuration can be measured with the same accuracy as for a single polarized antenna.

The antenna gain simulation contributes to a large amount to the total uncertainty. The investigation of the predicted resonance at 58 MHz indicate a much weaker influence of the metal pedestal than expected. The dip feature (Fig. 11) at the resonance frequency is introduced by the calculation of the amplification factors and does not appear during the investigation using a spherical antenna gain pattern. The present investigations have shown that the simulations used for the antenna gain have to be checked in greater detail to reveal the influence of the pedestal. Measurements with an increased coverage of the directional pattern can help to improve the simulations.

An important conclusion of this work is that the discussed strategy of calibration can be adapted for future radio antenna arrays measuring cosmic ray air showers. Especially at locations with much lower RFI an astronomical source, e.g. the galactic background radiation, can be used to cross-check the proposed amplitude calibration of a radio antenna system.

Acknowledgments

The authors would like to thank the technical staff of the Forschungszentrum Karlsruhe for their enthusiastic help during the calibration campaigns in the field, in particular Mr. Edgar Füssler, the crane driver, who always had fun and patience for the positioning of the reference source. Sincere thanks to the entire LOPES collaboration for providing the working environment for these studies.

References

[1] A. Haungs, H. Rebel, M. Roth, Rep. Prog. Phys. 66 (2003) 1145.
[2] W.E. Hazen, A.Z. Hendel, H. Smith, N.J. Shah, Phys. Rev. Lett. 22 (1969) 35.
[3] H.R. Allan, Prog. Elem. Part. Cosmic Ray Phys. 10 (1971) 171.
[4] V.B. Atrashkevich, et al., Sov. J. Nucl. Phys. 28 (1978) 3.
[5] H. Falcke, P. Gorham, Astropart. Phys. 19 (2003) 477.
[6] T. Huege, H. Falcke, Astropart. Phys. 24 (2003) 116.
[7] T. Huege, R. Engel, R. Ulrich, Astropart. Phys. 27 (2007) 392.
[8] A. Horneffer, LOPES Collaboration, et al., Int. J. Mod. Phys. A 21S1 (2006) 168.
[9] T. Antoni, KASCADE Collaboration, et al., Nucl. Instr. and Meth. A 513 (2003) 490.
[10] G. Navarra, KASCADE-Grande Collaboration, et al., Nucl. Instr. and Meth. A 518 (2004) 207.
[11] H.J.A. Röttgering, et al., astro-ph/0610596, 2006; H.J.A. Röttgering, New Astron. Rev. 47 (2003) 405.
[12] D. Ardouin, et al., Nucl. Instr. and Meth. A 555 (2005) 148.
[13] H. Gemmeke, LOPES Collaboration, et al., Int. J. Mod. Phys. A 21S1 (2006) 242.
[14] J. Abraham, Pierre Auger Collaboration, et al., Nucl. Instr. and Meth. A 523 (2004) 50.
[15] H. Falcke, LOPES Collaboration, et al., Nature 435 (2005) 313.
[16] A. Horneffer, Ph.D. Thesis, Rheinische Friedrich-Wihelms-Universität Bonn, Germany, 2006 ⟨http://nbn-resolving.de/urn:nbn:de:hbz:5N-07816⟩.
[17] W.D. Apel, LOPES Collaboration, et al., Astropart. Phys. 26 (2006) 332.
[18] S. Buitink, LOPES Collaboration, et al., Astron. Astrophys. 467 (2007) 385.
[19] J. Petrovic, LOPES Collaboration, et al., Astron. Astrophys. 462 (2007) 389.
[20] G.A. Dulk, et al., Astron. Astrophys. 365 (2001) 294.
[21] A. Nigl, et al., Astron. Astrophys. 471 (2007) 1099.
[22] A. Hakenjos, et al., LOPES Collaboration, Forschungszentrum Karlsruhe Report FZKA-7219, 2006.